Proc. Natl. Acad. Sci. USA
Vol. 96, pp. 8901–8906, August 1999
Biochemistry

Evolution of a light-harvesting protein by addition of new subunits and rearrangement of conserved elements: Crystal structure of a cryptophyte phycoerythrin at 1.63-Å resolution

KRYSTYNA E. WILK*†, STEPHEN J. HARROP*†, LUCY JANKOVA†, DIANA EDLER†, GARY KEENAN†, FRANCIS SHARPLES‡, ROGER G. HILLER‡, AND PAUL M. G. CURMI†§

†Initiative in Biomolecular Structure, School of Physics, University of New South Wales, Sydney, NSW 2052, Australia; and ‡School of Biological Sciences, Macquarie University, Sydney, NSW 2109, Australia

Communicated by Elisabeth Gantt, University of Maryland, College Park, MD, June 1, 1999 (received for review January 27, 1999)

ABSTRACT **Cryptophytes are unicellular photosynthetic algae that use a lumenally located light-harvesting system, which is distinct from the phycobilisome structure found in cyanobacteria and red algae. One of the key components of this system is water-soluble phycoerythrin (PE) 545 whose expression is enhanced by low light levels. The crystal structure of the heterodimeric $\alpha_1\alpha_2\beta\beta$ PE 545 from the marine cryptophyte *Rhodomonas CS24* has been determined at 1.63-Å resolution. Although the β-chain structure is similar to the α and β chains of other known phycobiliproteins, the overall structure of PE 545 is novel with the α chains forming a simple extended fold with an antiparallel β-ribbon followed by an α-helix. The two doubly linked $\beta50/\beta61$ chromophores (one on each β subunit) are in van der Waals contact, suggesting that exciton-coupling mechanisms may alter their spectral properties. Each α subunit carries a covalently linked 15,16-dihydrobiliverdin chromophore that is likely to be the final energy acceptor. The architecture of the heterodimer suggests that PE 545 may dock to an acceptor protein via a deep cleft and that energy may be transferred via this intermediary protein to the reaction center.**

Light-harvesting proteins increase the efficiency of photosynthetic organisms growing in low-light regimes. They act as antennae, capturing photons over a broad frequency spectrum and transferring energy to membrane-bound reaction centers (1). In cyanobacteria and red algae, the light-harvesting phycobiliproteins (PBPs) are water soluble and organized into phycobilisomes (large, multiprotein complexes bound to the stromal face of the thylakoids). Individual PBPs and phycobilisomes have been studied by x-ray crystallography (2–11) and electron microscopy (12, 13) as well as biochemically (14). The individual proteins are structurally conserved with a basic $\alpha\beta$ unit (referred to by convention as monomer) arranged around a 3-fold axis forming an $(\alpha\beta)_3$ trimer. Cryptophyte algae also use PBPs to harvest light but these differ from those of the cyanobacteria and red algae in several significant ways (15). In any one species, there is only one type of PBP, either phycocyanin (PC) or phycoerythrin (PE); allophycocyanin is never present. The PC or PE is not organized into a phycobilisome but is instead located in the thylakoid lumen (16–18). Although the β subunits of cryptophyte PBPs share a high degree of sequence identity with both the α and β subunits of cyanobacterial and red algal PBPs (19), the α subunits are shorter, unrelated to other proteins in the sequence databases and carry a single, spectroscopically distinct bilin chromophore (20, 21). Structurally, they also differ in being $\alpha_1\alpha_2\beta\beta$ dimers rather than $(\alpha\beta)_3$ trimers. We report here the structure at 1.63 Å of PE 545 from the marine cryptophyte *Rhodomonas* (formerly *Chroomonas*) *CS24*.

METHODS

Protein Preparation and Crystallization. PE 545 was purified (22) from *Rhodomonas CS24* (Commonwealth Scientific and Industrial Research Organization, Division of Fisheries, Hobart, Australia) with additional ion exchange (POROS 20HQ) and size exclusion (BioSep-SEC-S1000) chromatography. Both columns were equilibrated in 50 mM Mes, pH 6.5 with 0.5 mM NaN_3. PE 545 was eluted from the ion exchange column by using a 0–1 M NaCl gradient. Crystals of PE 545 grew readily over a range of conditions with polyethylene glycol (PEG) as the precipitant (compare with PE 545 from *Rhodomonas* lens; ref. 23). Single crystals ($1 \times 0.5 \times 0.5$ mm^3) of space group $P2_12_12_1$ with lattice dimensions of 63.3 Å × 83.8 Å × 90.7 Å were grown by sitting drop vapor diffusion. The crystallization solution contained 20% PEG 4K, 100 mM $MgCl_2$, 50 mM LiCl, and 50 mM Tris at pH 8.5. Five microliters of 20 mg ml^{-1} PE 545 in 50 mM Mes, pH 6.5 was mixed with 5 μl of reservoir solution and equilibrated at room temperature. Crystals appeared within 2 weeks.

Data Collection and Structure Determination. Diffraction data were collected on a Macscience (Nonius BV, Delft The Netherlands) DIP2030 imaging plate detector mounted on a Nonius Cu rotating anode generator with focusing mirrors. Crystals were flash-frozen in a stream of nitrogen at 100 K after soaking in a cryoprotection buffer. Data were processed by using the programs DENZO and SCALEPACK (24). Initial phases were determined by using the β subunits of the phycobilisome PE from *Polysiphonica urceolata* (1LIA; ref. 10) as a molecular replacement probe. Rotation and translation functions calculated by using the CCP4 (25) program AMORE (26) gave two strong solutions, which were consistent with the solution to the self-rotation function. These models provided approximately 40% of the scattering mass. A free atom refinement approach was used to improve the phases (implemented by using the program ARP; ref. 27). A set of atoms was added to the model, and all atoms were refined by ARP. At the end of a cycle, all atoms were tested for correlation to the electron density, and atoms with poor correlations were rejected. The top 100 peaks containing no atoms were assigned atoms. The refinement cycle then was repeated and the whole

The publication costs of this article were defrayed in part by page charge payment. This article must therefore be hereby marked "*advertisement*" in accordance with 18 U.S.C. §1734 solely to indicate this fact.

PNAS is available online at www.pnas.org.

Abbreviations: PE, phycoerythrin; PBP, phycobiliprotein; PEB, phycoerythrobilin; DBV, 15,16-dihydrobiliverdin.

Data deposition: The coordinates have been deposited in the Protein Data Bank, www.rcsb.org (PDB ID code 1qgw).

*K.E.W. and S.J.H. contributed equally to this work.
§To whom reprint requests should be addressed. E-mail: P.Curmi@unsw.edu.au.

Table 1. Data collection and refinement statistics

Number of crystals	1
Number of measured reflections	264,395
Number of unique reflections	56,582
Maximum resolution	1.63 Å
Completeness of data (1.67–1.63 Å shell)	95.8 (79.4)
I/σ (1.67–1.63 Å shell)	21.3 (12.0)
R_{merge}(1.67–1.63 Å shell)	0.039 (0.104)
Number of protein atoms	3,574
Number of chromophore atoms	344
Number of water molecules	833
Crystallographic *R* factor	0.149
R_{free}	0.188
rms deviation bond lengths*	0.007 Å
rms deviation bond angles*	1.1°
Ramachandran plot*	
Most favored region	93.4%
Additionally allowed	6.1%
Disallowed	0.5%

*From PROCHECK (43).

process continued until convergence. The final map showed readily interpretable electron density for the two α subunits and the chromophores that were not included in the initial phasing model. The model was built by using the program O (28) and refined by maximum-likelihood methods using the CCP4 (25) program REFMAC (29). All expected protein residues are in unambiguous electron density with the exception of the N terminus of β subunit C where clear density for residues 1, 2, and 10–15 was absent. (We have labeled the β subunits C and D, indicating that they are intimately linked to the α_1 and the α_2 subunits to form the two $\alpha\beta$ monomers, respectively.) The final model (which excluded residues 1, 2, and 10–15 of β subunit C) gave an *R* factor of 0.15 with an R_{free} of 0.19. Table 1 presents the data reduction and refinement statistics. The model shows high stereochemical quality with the only outlier on the Ramachandran plot being Thr-75 in both β subunits. The unusual geometry of Thr-75 is common to all PBPs (2–10).

Energy Transfer Parameters. Energy transfer rates, k_{et}, for chromophore pairs were calculated by using the Förster equation (30) where chromophore separations and orientation factors were determined as per PBPs (9) by using a Förster distance of 50 Å and a fluorescence lifetime of 2.7 ns for all chromophores.

RESULTS

Structure. The PE 545 $\alpha_1\alpha_2\beta\beta$ dimer forms a boat-shaped molecule (approximately 75 Å × 60 Å × 40 Å). A C_α tracing of the dimer, which forms the asymmetric unit of our crystal form, is shown in Fig. 1*A*. The β subunits are similar to each other and both α and β subunits of the PBPs (2–10), forming part of the globin family of protein structures (Fig. 2*A*). The major differences between the two β subunits, and among the members of PBP family, are in the N-terminal regions, including helices X and Y that are separate from the main body, and in the GH loop (2–10). Least-squares alignment of the two PE 545 β subunits gives a rms deviation D of 0.6 Å (over 161 C_α atoms) compared with 0.7 and 0.8 Å for the two β subunits (C over 144 and D over 140 C_α atoms, respectively) aligned to the phycobilisome PE β subunit (10).

The α subunits consist of an antiparallel β-ribbon followed by an α-helix (Figs. 1 and 2). Each α subunit is extended along its respective β subunit. The α subunits are not identical as expected from previously determined sequence differences (22, 31, 32). We observe two α subunits, α_1 and α_2, respectively (Figs. 1 and 2) with the major sequence and structural differences residing in the C-terminal regions; α_1 is longer than α_2 (76 versus 67 residues) and the C-terminal extension of α_1 is important in chromophore binding (Fig. 3*A*). The C-terminal helix in the α_2 subunit is longer than that in α_1 (Fig. 2*D*). Both α subunit C termini are approximately in the same position with respect to their β subunits. Our electron density maps

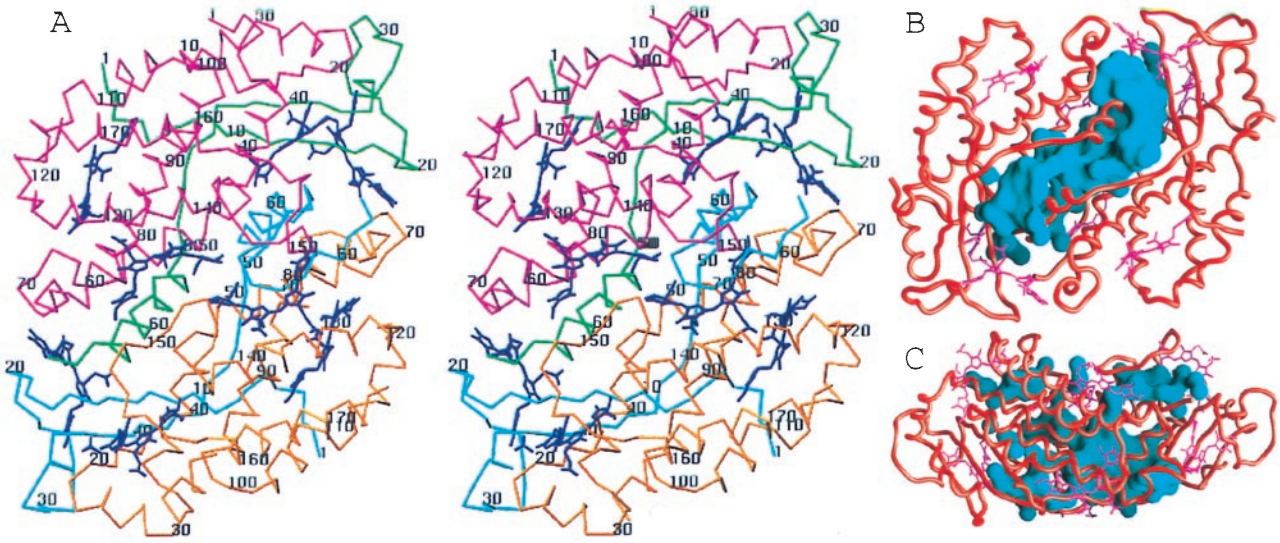

FIG. 1. C_α tracing of the PE 545 dimer plus two views of the polar slot. (*A*) A stereo Cα diagram of the PE 545 dimer showing all of the chromophores (α_1 cyan, α_2 green, β chains gold and magenta, and chromophores blue). The view is down the pseudo 2-fold axis. The pair of β50/β61 chromophores is toward the viewer, just covered by loops from the α_1 and β chains. *A* was produced with the program SETOR (42). (*B* and *C*) The solvent-filled slot that separates the two $\alpha\beta$ monomers is shown as a molecular surface (blue). (*B*) The view is down the pseudo 2-fold axis from the face opposite the one containing the two β50/β61 chromophores. The backbone is shown as a red tube. The α19 subunit helices can be seen entering the edges of the slot. The monomer on the left is $\alpha_2\beta$ while $\alpha_1\beta$ is on the right. Note that the slot is wider in the upper half because of the flat face of the C-terminal helix of the α_2 subunit. The chromophores are shown in pink. The α19 chromophores are at the interface between the two monomers, bounding the ends of the slot. (*C*) An orthogonal view where the β50/β61chromophores are on the top surface near the center. The slot enters from the bottom and is not symmetric about the pseudo 2-fold axis (running up the page). The α19 chromophores are at the bottom left and right demarcating the ends of the slot. *B* and *C* were produced by using the program GRASP (35).

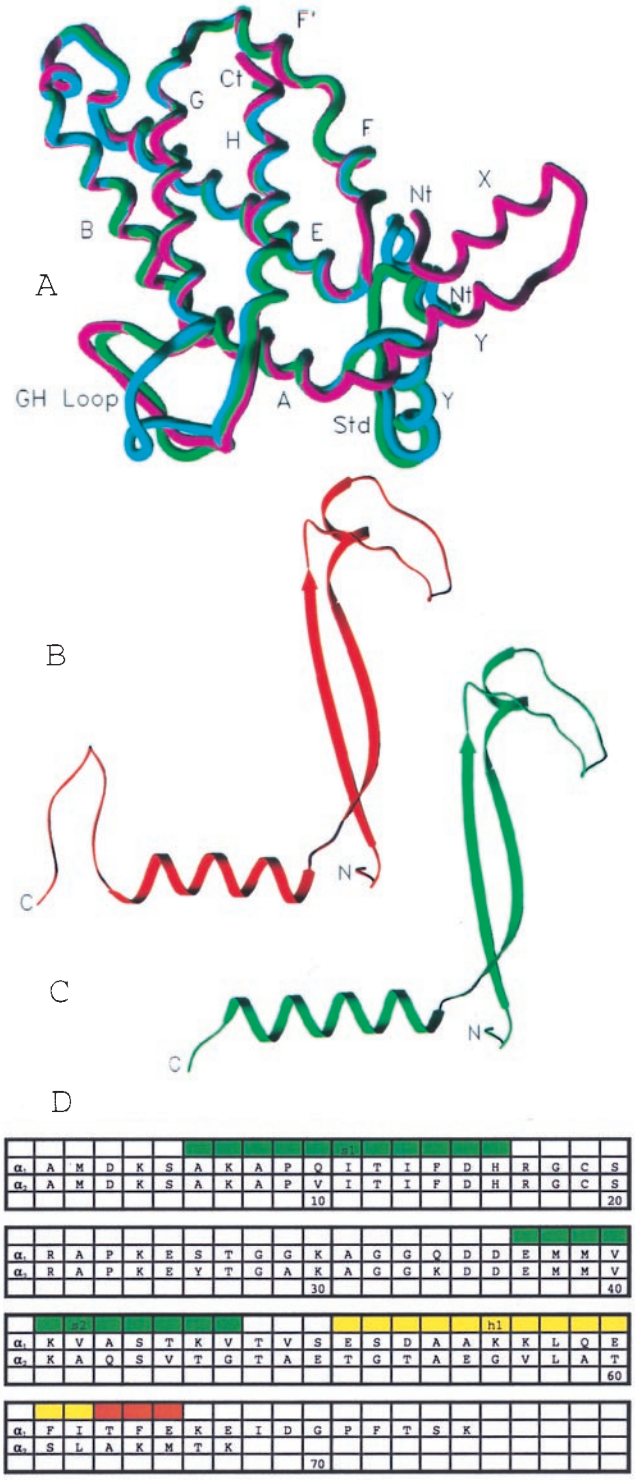

FIG. 2. Subunit secondary structures and sequences. (*A*) A superposition of β subunit C (blue), β subunit D (green) with the phycobilisome PE β subunit (red; ref. 10). Helices are labeled X, Y, A, B, E, F, F′, G, and H. All C termini are at one location, Ct, and the distinct N termini are labeled Nt. (*B* and *C*) Ribbon representations of the α_1 (red) and α_2 (green) subunits, respectively. (*D*) The aligned sequences of the α subunits along with the secondary structure. The green bars indicate β-strands 1 and 2. The yellow bar indicates the α-helix in the α_1 chain. The helix in the α_2 chain is longer by three residues (shown in red).

show no evidence for the reported heterogeneity in cryptophyte dimers caused by the α subunits (22, 32, 33).

A unique feature of our PE 545 structure is the presence of a β-sheet, as all other structures of PBPs are devoid of β-sheet structure (2–10) with the exception of the linker polypeptide (11). In our dimer, there are two nearly identical β-sheets, each composed of two strands from an α subunit plus one strand from its partner β subunit. The portion of the β subunit that forms the third β-strand is part of the N-terminal extension of the standard globin fold.

Two ions were clearly identified in the structure. The electron density for a Mg^{2+} ion octahedrally coordinated by six water molecules was observed at the C terminus of the α-helix in the α_1 subunit. The electron density, coordination geometry, and correlation between the *B* factors of the ion and its oxygen ligands support our assignment. A second ion was identified as a Cl^- ion (Fig. 3*A*), which coordinated one of the pyrrole nitrogens in the $\beta 50/\beta 61$ chromophore in β subunit D. The coordination shell of the Cl^- is completed by the OH of Ser-147 and the side chain NH of Gln-148 from the GH loop of β subunit D, as well as a water ligand (Fig. 3*A*). This Cl^- ion was identified by the fact that it showed extra electron density in difference maps and its *B* factor dropped to 2 $Å^2$ during each refinement cycle (compared to > 5 $Å^2$ for typical water molecules). In addition, it gave a 7-σ peak in an anomalous Fourier map. We note that both of these ions could result simply from the 0.1 M $MgCl_2$ present in the crystallization solution.

Two posttranslationally modified residues per monomer were identified in the electron density map. As expected, residue 72 in the β subunit is a γ-*N*-methylasparagine, a modification conserved in most PBPs (34). Lys-4 in both α subunits also appears to be modified, with the electron density and chemical environment being consistent with 5-hydroxyllysine. Both modified residues are in the vicinity of the $\beta 82$ chromophore (Fig. 3*B*).

Quaternary Structure. The PE 545 dimer is formed by the association of two tightly linked $\alpha\beta$ monomers (Fig. 1*A*). Within the monomer, the α chain makes intimate contacts with the β chain via the formation of the β-sheet and via the packing of the α chain helix against helices B and E of the β subunit. The formation of the $\alpha_1\beta$ and $\alpha_2\beta$ monomers results in the burial of 4,900 $Å^2$ and 4,300 $Å^2$ of accessible surface area (35), respectively. The assembly of the two monomers into the dimer results in the burial of an additional 4,000 $Å^2$ of accessible surface area and is commensurate with the stability of the dimer (36). We note that the computed buried accessible surface area on dimer formation is an overestimate because of the difficulties posed by the presence of a deep polar slot.

The interface between the two $\alpha\beta$ monomers is unusual in that it is very polar and highly solvated (hence the high proportion of ordered water molecules, Table 1). Intimate contacts between the monomers primarily are formed in the vicinity of the $\alpha 19$ chromophores and the $\beta 50/\beta 61$ chromophores, the latter being in van der Waals contact at the interface between monomers (Fig. 3*A*). Almost all protein–protein contacts between the two monomers are mediated through the α subunits, and the only contact between the two β subunits is in the vicinity of the two $\beta 50/\beta 61$ chromophores.

Polar Slot. A striking feature of the dimer is the cavity filled with ordered water molecules that forms a slot between the two monomers (Fig. 1 *B* and *C*). The slot enters the dimer parallel to the pseudo 2-fold axis relating the two monomers. The slot is approximately 15 Å deep and 20 Å long while its width varies from 5 to 10 Å. Its shape is asymmetric because of the sequence differences between the C-terminal helices of the α subunits. In particular, the C-terminal helix of the α_2 subunit presents a flat face to the slot because of the presence of Gly-52, Gly-56, Ala-59, and Ala-63. There are continuous chains of hydrogen-bonded water molecules that pass all the way through the dimer (Fig. 1*C*). The slot is reminiscent of a docking site for a peptide or other medium-sized molecule that may interact with PE 545.

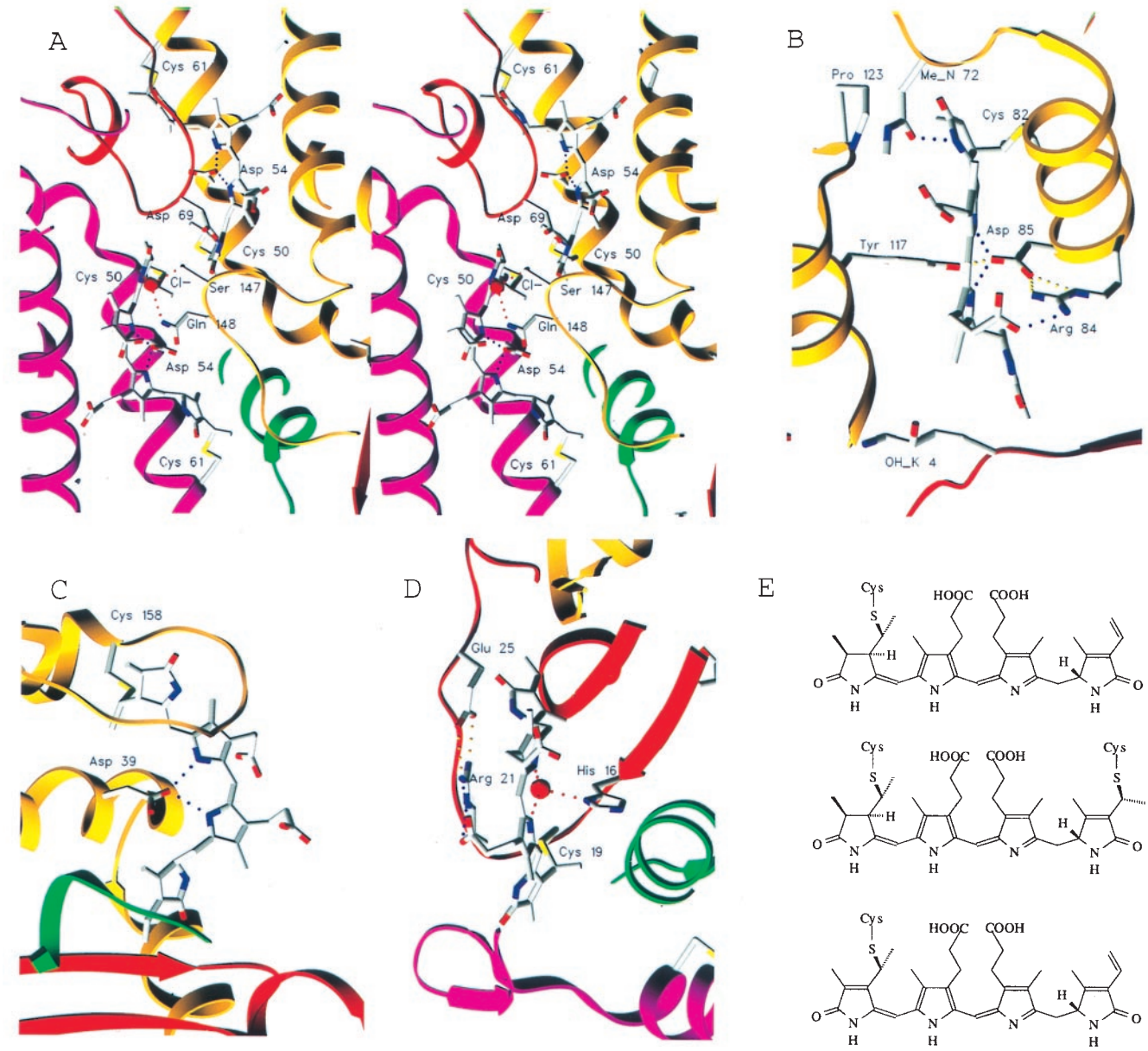

FIG. 3. Representative chromophore sites for PE 545. The subunits are color-coded with α_1 red, α_2 green, β subunit C gold, and β subunit D magenta. (*A*) A stereo view of the two $\beta 50/\beta 61$ chromophores looking down the pseudo 2-fold axis. The two chromophores lie along their respective B helices. Pyrrole ring A of each chromophore is in van der Waals contact with its opposite. In each chromophore, the pyrrole nitrogen of the A ring is coordinated by a negative charge. In one case, it is Asp-69 form the $\alpha 1$ chromophore; in the other case, it is a Cl^- ion (red sphere). There is an asymmetric arrangement of protein loops interacting with these chromophores. On the lower right, the loop linking helices G and H (gold) interacts with the two chromophores; on the upper left, the loop extending from the C terminus of the α_1 subunit (red) has displaced the β G-H subunit loop and it interacts with the chromophores. (*B*) The $\beta 82$ chromophore that is wrapped around helix E (upper right). It interacts with a cluster of residues that are highly conserved in the PBPs (Cys-82, Arg-84, Asp-85, and Tyr-117). Two posttranslationally modified residues [*N*-methylasparagine 72 (Me_N) and 5-hydroxylysine 4 (OH_K)] are proximal to this chromophore. (*C*) The $\beta 158$ chromophore is covalently attached to Cys-158 on helix H while being wrapped around helix A (center left). (*D*) The $\alpha_1 19$ chromophore is at the junction of all four protein chains (as is the $\alpha_2 19$ chromophore). The nitrogen atoms of the two central pyrrole rings are coordinated by a water molecule (red sphere). This is hydrogen-bonded to His-16 and another water molecule (not shown). Glu-25 coordinates the nitrogen atom of pyrrole ring D. The $\alpha 19$ chromophores differ from the β chromophores in that pyrrole A has been oxidized so that all atoms attached to it are coplanar with the ring (bottom). (*E*) The chemical structures of the three types of chromophores observed in the PE 545 structure. (*Top*) The standard PE chromophore as per $\beta 82$ and $\beta 158$; (*Middle*) the doubly linked $\beta 50/\beta 61$ chromophore; and (*Bottom*) the $\alpha 19$ DBV chromophore. It differs from the PE chromophores in that the A pyrrole ring is fully conjugated. In each schematic, the pyrrole rings are A, B, C, and D, from left to right.

Comparison to Phycobilisome Proteins. We have overlayed the PE 545 $\alpha_1\alpha_2\beta\beta$ dimer on the $(\alpha\beta)_6$ hexamer structure that forms the basis of the phycobilisome (3). The overlay of the PE 545 β subunit with the phycobilisome β subunit results in overwhelming steric clashes between the PE 545 dimer and the hexamer. Overlaying the PE 545 β subunit with the phycobilisome α subunit results in minimal clashes between the PE 545 dimer and the phycobilisome hexamer. We conclude that the subunit interactions within the PE 545 dimer is unlikely to participate in a higher-order aggregate that resembles the phycobilisome structure.

Recently, the structure of a PBP has been determined that includes the linker polypeptide L_C[7,8], which is one of the proteins responsible for the strict sequential assembly of the phycobilisomes (11). Like the α subunit of PE 545, the linker polypeptide is small (67 residues) and unlikely to have a

Table 2. Energy transfer parameters

	$\alpha_1$19	$\alpha_2$19	β50/β61C	β82C	β158C	β50/β861D	β82D
$\alpha_2$19	44.5						
	0.2						
β50/β61C	29.2	24.0					
	0.7	**36**					
β82C	34.7	21.5	21.5				
	2.0	**43**	**66**				
β158C	21.8	45.3	22.0	35.6			
	6.7	0.4	**26**	2.9			
β50/β61D	23.3	28.5	12.4	29.3	22.4		
	41	0.1	**2,600**	**20**	6.3		
β82D	21.4	34.8	30.5	35.2	36.6	21.3	
	85	2.2	**14**	0.2	0.3	**45**	
β158D	44.7	21.0	21.5	35.4	40.5	21.6	35.4
	0.3	1.7	4.0	0.04	2.2	**10**	3.0

Listed are the distance between the chromophores (Å) and the estimated Förster energy transfer rate, k_{et} (ns^{-1}). Transfer rates greater than 10 ns^{-1} are in bold.

tertiary structure in the absence of interactions with the PBPs (11). $L_C^{7.8}$ bears an uncanny resemblance to the PE 545 α subunit as it consists of a three-stranded β-sheet plus an α-helix. However, the architectures of the PE 545 α subunit and $L_C^{7.8}$ are distinct and there is no apparent sequence similarity between the two, even after structural alignment of the N-terminal β-hairpin. The interactions between $L_C^{7.8}$ and its PBPs are different from the interactions between the PE 545 subunits.

Chromophores. Three chromophores are linked to each β subunit whereas one chromophore is linked to each α subunit. The three β subunit chromophores, β50/β61, β82, and β158, are phycoerythrobilins (PEBs; Fig. 3*E*). Each has an aspartic acid side chain coordinating the nitrogen atoms of the central two pyrrole rings. The acidic coordination is observed in all other reported PBP structures (2–10).

The β82 chromophore, which is common to all PBPs, is located in a pocket formed by helices E and F′ (heme pocket in globins; ref. 2) and the N terminus of the α subunit (Fig. 3*B*). Asp-85, which coordinates the central pyrrole nitrogens, is salt-linked to Arg-84, which also is linked to the propionate attached to the C ring of the chromophore. These residues are conserved in more than 90% of PBPs. Note the presence of the two modified amino acids in the vicinity of the chromophore (Fig. 3*B*). In a similar fashion, the β158 chromophore is attached to the loop linking helices G and H (Fig. 3*C*) with Asp-39 coordinating the nitrogen atoms of the two central pyrroles.

The doubly linked β50/β61 chromophore is extended along the length of helix B, to which it is covalently attached by Cys-50 and Cys-61 (Fig. 3*A*). The nitrogen atoms of the two central pyrroles are coordinated by the side chain of Asp-54. This chromophore differs from the other two on the β subunit in at least three ways: it has two covalent linkages, the nitrogen of pyrrole A has a negatively charged ligand, and two β50/β61 chromophores are in van der Waals contact with each other across the pseudo 2-fold axis that relates the two halves of the $\alpha_1\alpha_2\beta\beta$ dimer (Figs. 1*A* and 3*A*). Their A pyrrole rings are stacked in a staggered fashion with their conjugated rings essentially parallel to each other and in contact. Of all the chromophores in PBPs whose structures have been determined (2–10), this pair of β50/β61 chromophores is the only one in such close proximity.

On β chain C, the nitrogen of pyrrole A of β50/β61 is coordinated by the side chain of Asp-69 from the α_1 subunit, which is part of the same monomer (Fig. 3*A*). Such a coordination is not possible for the β50/β61 chromophore attached to β subunit D, because of the asymmetry in α subunits. In our structure, a chloride ion is coordinating the pyrrole in place of the aspartate side chain. This need for a second negatively charged ligand on the two β50/β61 chromophores is likely to have implications for their physical state and spectroscopic properties.

The chromophores linked to the α subunit are chemically distinct from the β subunit PEB chromophores (Fig. 3 *D* and *E*). Our structure is consistent with the presence of a singly linked 15,16-dihydrobiliverdin (DBV) chromophore as determined previously by NMR and MS (21). This chromophore differs from PEB in that pyrrole A is oxidized so that all atoms within the ring are in an sp2 state (Fig. 3 *D* and *E*) with the result that all atoms attached to pyrrole A are coplanar with the pyrrole ring.

The ligands attached to the nitrogen atoms in the α19 chromophore also differ from those of the β subunit PEB chromophores, as nitrogen atoms in the two central pyrroles are coordinated by a water molecule (Fig. 3*D*), which, in turn, is coordinated by His-16 of the respective α subunit and another water molecule. Consequently, there is no negatively charged ligand at this central coordination site, distinguishing the α19 chromophore from all other phycobilin structures (2–10). Also, in contrast to the β subunit PEB chromophores, the nitrogen atom of pyrrole D is coordinated to the side chain of Glu-25 of its respective α subunit (Fig. 3*D*).

The additional conjugation of the α19 chromophore compared with that of the PEBs alters its spectral properties, moving the absorption maximum of DBV to 562 nm (compared with 550 nm for PEB; ref. 21). Thus, it is a likely candidate for the final photon energy acceptor in this form of PE 545 (i.e., the point at which all photon energy arrives before transfer to a chromophore of an acceptor protein). Its location near the polar slot may be of functional significance.

Implications for Light Harvesting. All the chromophores in this PE 545 structure are in close proximity (<45 Å between centers of mass of the conjugated atoms). Calculation of energy transfer parameters for all possible pairs of chromophores in the $\alpha_1\alpha_2\beta\beta$ dimer, assuming Förster resonance dipole–dipole coupling, indicates that 11 of the 28 chromophore pairs have calculated transfer rates, k_{et}, exceeding 10 ns^{-1} (Table 2), which is rapid compared with the lifetime of the PEB excited state, τ_o = 2.7 ns. Thus, energy will rapidly migrate through the network of chromophores to the terminal acceptors.

The central β50/β61 chromophores have a separation of 12.4 Å with favorable stacking of their A pyrrole rings. It is possible that they possess a strong exciton interaction, which may alter their chromophoric properties. In contrast, the two β158 chromophores are the most isolated in terms of energy transfer. They only participate in one pairing with $k_{et} > 10$ ns^{-1}, which is with their respective β50/β61 chromophores. Each α19 chromophore appears to be coupled with the β82

and $\beta 50/\beta 61$ chromophores from its opposite β subunit, with the two β-chromophores coupled to each other.

DISCUSSION

The structure of PE 545 demonstrates the evolution of a functional protein complex based on the rearrangement of related elements (from phycobilisome PBPs) and the addition of new subunits that are unlikely to fold in isolation. As such, it is important to examine how the new arrangement alters the properties of the light-harvesting unit. PE 545 has several new features that include the contacting $\beta 50/\beta 61$ chromophore pair, the α subunits with their DBV chromophores, and the inter-monomer slot. These may hold clues as to how the cryptophyte light-harvesting system operates.

The PE 545 dimer has been studied by biochemical and spectroscopic techniques (36). The dimeric form was shown to be stable, requiring nonbiological conditions to produce the monomer. Dissociation into the monomer resulted in the reduction of the absorbance at 550 nm by approximately 20% and a drop in the positive and negative CD bands at 540 and 580 nm by about 1/3. Two photon fluorescence lifetime measurements showed that monomerization resulted in the loss of the fastest lifetime measured (2.4 ps increasing to 40 ps in the monomer). The structure indicates that these changes are likely to be caused by the separation of the pair of $\beta 50/\beta 61$ chromophores, which is consistent with the proposal that the change in CD is the result of the disruption of a pair of chromophores that are exciton-coupled in the dimer (36). However, the persistence of positive and negative CD bands in the monomer indicates that the chromophores within the monomer are also exciton-coupled, but this coupling is not immediately obvious from the structure. Combining these findings, it appears that the most significant advantage of the dimeric form is the presence of extremely rapid energy transfer between the two monomers, which is mediated by the pair of $\beta 50/\beta 61$ chromophores.

The $\alpha 19$ chromophore (DBV) is the most likely candidate for the final acceptor on PE 545. This arrangement is true for the most cryptophyte PBPs (21) with some exceptions (37). The question remains as to how this energy then is transferred to the chlorophylls of the reaction center. Based on steady-state fluorescence measurements, it has been suggested that energy transfer is primarily to photosystem II (PSII) as in the phycobilisome (38, 39). However, attempts to isolate and characterize a PE-PSII particle have not shown clear coupling between these components.

In the PE 545 structure reported here the large cavity containing bound water could be a site for interaction with a component of photosystem II (PSII) that protrudes into the thylakoid lumen. Possible candidates include the inner antennae of PSII, Cp43, and Cp47. However, the sequences of Cp43 (psbC) and Cp47 (psbB) for the cryptophyte, *Guillardia theta,* show no evidence of new features that might imply unique binding sites for PE (40). Time-resolved fluorescence emission demonstrated that PE 565 in *Cryptomonas CR1* transferred its energy, possibly via a 655-nm component, to chlorophyll 682, which was assigned to the intrinsic integral membrane light-harvesting complex (LHC) and subsequently to Cp43/Cp47 (41). Thus, cryptophyte PE may interact directly with LHC or possibly the 655-nm component protein. It is possible that these putative interactions are mediated by the polar slot.

This project has been supported by Australian Research Council project and Research Infrastructure Equipment and Facilities Project grants.

1. Larkum, T. & Howe, C. J. (1997) *Adv. Bot. Res.* **27,** 257–330.
2. Schirmer, T., Bode, W., Huber, R., Sidler, W. & Zuber, H. (1985) *J. Mol. Biol.* **184,** 257–277.
3. Schirmer, T., Huber, R., Schneider, M., Bode, W., Miller, M. & Hackert, M. L. (1986) *J. Mol. Biol.* **188,** 651–676.
4. Schirmer, T., Bode, W. & Huber, R. (1987) *J. Mol. Biol.* **196,** 667–695.
5. Duerring, M., Huber, R., Bode, W., Reumbeli, R. & Zuber, H. (1990) *J. Mol. Biol.* **211,** 633–644.
6. Duerring, M., Schmidt, G. B. & Huber, R. (1991) *J. Mol. Biol.* **217,** 577–592.
7. Ficner, R., Lobeck, K., Schmidt, G. & Huber, R. (1992) *J. Mol. Biol.* **228,** 935–950.
8. Ficner, R. & Huber, R. (1993) *Eur. J. Biochem.* **218,** 103–106.
9. Brejc, K., Ficner, R., Huber, R. & Steinbacher, S. (1995) *J. Mol. Biol.* **249,** 424–440.
10. Chang, W., Jiang, T., Wan, Z., Zhang, J., Yang, Z. & Liang, D. (1996) *J. Mol. Biol.* **262,** 721–731.
11. Reuter, W., Wiegand, G., Huber, R. & Than, M. E. (1999) *Proc. Natl. Acad. Sci. USA* **96,** 1363–1368.
12. Morschel, E. & Rhiel, E. (1987) in *Electron Microscopy of Proteins*, eds. Harris, J. R. & Horne, R. W. (Academic, New York) Vol. 6, pp. 209–554.
13. Lage, W., Wilhelm, C., Wehrmeyer, W. & Morschel, E. (1990) *Bot. Acta* **103,** 250–257.
14. Glazer, A. N. (1985) *Biochim. Biophys. Acta* **768,** 29–51.
15. MacColl, R. & Guard-Friar, D. (1987) *Phycobiliproteins* (CRC, Boca Raton, FL).
16. Gantt, E., Edwards, M. R. & Provasoli, L. (1971) *J. Cell Biol.* **48,** 280–290.
17. Spear-Bernstein, L. & Miller, K. R. (1989) *J. Phycol.* **25,** 412–419.
18. Vesk, M., Dwarte, D., Fowler, S. & Hiller, R. G. (1992) *Protoplasma* **170,** 166–176.
19. Apt, K. E., Collier, J. L. & Grossman, A. R. (1995) *J. Mol. Biol.* **248,** 79–96.
20. Guard-Friar, D. & MacColl, R. (1986) *Photochem. Photobiol.* **43,** 81–85.
21. Wedemayer, G. J., Kidd, D. G., Wemmer, D. E. & Glazer, A. N. (1992) *J. Biol. Chem.* **267,** 7315–7331.
22. Martin, C. D. & Hiller, R. G. (1987) *Biochim. Biophys. Acta* **923,** 88–97.
23. Becker, M., Studds, M. T. & Huber, R. (1998) *Protein Sci.* **7,** 580–586.
24. Otwinowski, Z. & Minor, W. (1997) *Methods Enzymol.* **276,** 307–326.
25. Collaborative Computing Project No. 4 (1994) *Acta Crystallogr. D* **50,** 760–763.
26. Navaza, J. (1994) *Acta Crystallogr. D* **50,** 157–163.
27. Lamzin, V. S. & Wilson, K. S. (1993) *Acta Crystallogr. D* **49,** 129–147.
28. Jones, T. A., Zou, J. Y., Cowan, S. W. & Kjeldgaard, M. (1991) *Acta Crystallogr. A* **47,** 110–119.
29. Murshudov, G. N., Vagin, A. A. & Dodson, E. J. (1997) *Acta Crystallogr. D* **53,** 240–255.
30. Förster, T. (1965) in *Modern Quantum Chemistry*, ed. Sinanoglu, O. (Academic, New York) Part III, pp. 93–97.
31. Sidler, W., Kumpf, B., Frank, G., Suter, F., Morriset, W., Wehrmeyer, W. & Zuber, H. (1985) *Hoppe-Zeylers Z. Physiol. Chem.* **366,** 233–244.
32. Jenkins, J. J., Hiller, R. G., Speirs, J. & Godovac-Zimmermann, J. (1990) *FEBS Lett.* **273,** 191–194.
33. Morschel, E. & Wehrmeyer, W. (1977) *Arch. Microbiol.* **113,** 83–89.
34. Klotz, A. V., Leary, J. A. & Glazer, A. N. (1986) *J. Biol. Chem.* **261,** 15891–15894.
35. Nicholls, A., Bharadwaj, R. & Honig, B. (1993) *Biophys. J.* **64,** 166–170.
36. MacColl, R., Malak, H., Gryczynski, I., Eisele, L. E., Mizejewski, G. J., Franklin, E., Sheikh, H., Montellese, D., Hopkins, S. & MacColl, L. C. (1998) *Biochemistry* **37,** 417–423.
37. Wemmer, D. E., Wedemayer, G. J. & Glazer, A. N. (1993) *J. Biol. Chem.* **268,** 1658–1669.
38. Lichtlé, C., Jupin, H. & Duval, J. C. (1980) *Biochim. Biophys. Acta* **591,** 104–112.
39. Lichtlé, C., Duval, J. C. & Lemoine, Y. (1987) *Biochim. Biophys. Acta* **894,** 76–90.
40. Douglas, S. E. & Penny, S. L. (1999) *J. Mol. Evol.* **48,** 236–244.
41. Mimuro, M., Tamai, N., Murakami, A., Watanabe, M., Erata, M., Watanabe, M., Tokutomi, M. & Yanazaki, I. (1998) *Phycol. Res.* **46,** 155–164.
42. Evans, S. V. (1993) *J. Mol. Graphics* **11,** 134–138.
43. Laskowski, R. A., MacArthur, M. W., Moss, D. S. & Thornton, J. M. (1994) *J. Appl. Crystallogr.* **26,** 283–291.